Chem

CellPress

Article

An aqueous artificial molecular pump

Christopher K. Lee,[1] Yuanning Feng,[2,*] Alan E. Enciso,[3] Jake P. Violi,[1] William A. Donald,[1] J. Fraser Stoddart,[1,3,4,5,6,7,8] and Dong Jun Kim[1,9,*]

[1]School of Chemistry, University of New South Wales, Sydney, NSW 2052, Australia
[2]Department of Chemistry and Biochemistry, The University of Oklahoma, Norman, OK 73019, USA
[3]Weinberg College of Arts and Sciences, Northwestern University, Evanston, IL 60208, USA
[4]Department of Chemistry, The University of Hong Kong Hong Kong 999077, Hong Kong SAR, China
[5]Center for Regenerative Nanomedicine, Northwestern University, Chicago, IL 60611, USA
[6]Stoddart Institute of Molecular Science, Department of Chemistry, Zhejiang University, Hangzhou 310027, Zhejiang, China
[7]ZJU-Hangzhou Global Scientific and Technological Innovation Center, Hangzhou 311215, Zhejiang, China
[8]Deceased, December 30, 2024
[9]Lead contact
*Correspondence: yf@ou.edu (Y.F.), dongjun.kim@unsw.edu.au (D.J.K.)
https://doi.org/10.1016/j.chempr.2025.102693

THE BIGGER PICTURE Molecular machines power many fundamental biological processes. These biological machines operate exclusively in water. In contrast, almost all artificial molecular machines have been designed to function in organic solvents, with only a rare few reported in aqueous environments. This disconnect between nature and the laboratory means that while synthetic molecular machines are biologically inspired, their behavior under biologically relevant conditions is poorly understood. Artificial molecular pumps are a growing family of molecular machines capable of driving away from equilibrium transport. The use of these pumps in water, however, has not been described previously. Herein, we report the preparation of such a pump and demonstrate its rapid and efficient operation in water. This research helps to bridge the gap between biological and artificial molecular machinery, paving the way for the integration of these machines into bioinspired systems, perhaps even into synthetic cells.

SUMMARY

This work presents an artificial molecular pump designed for efficient operation in water, advancing the integration of synthetic molecular machines into biologically relevant environments. The pump function, demonstrated through the formation of [2]- and [3]rotaxanes, exhibits enhanced efficiency and faster kinetics compared with analogous systems in organic solvents. These improvements stem from radical-radical interactions amplified by water due to its high polarity, emphasizing the solvent's role in molecular machine performance. The findings underscore the ability of water to strengthen supramolecular interactions essential for pump operation, providing a framework for designing next-generation molecular machines capable of functioning under more biochemically relevant conditions.

INTRODUCTION

In nature, many key functions of cells are driven by a complex array of nanoscale machines.[1] These biological machines are structures that have been fine-tuned by evolution to move in precise fashion in response to environmental stimuli.[2] These mechanical movements are used to drive and maintain the complex biochemistry necessary for life.[1,2] Biological molecular pumps are one class of these machines, which are responsible for the maintenance of concentration gradients by consuming energy and transporting chemical species from areas of lower concentration to areas of higher concentration.[3,4] For example, the sodium-potassium pump (NaK-ATPase) is an enzyme that imports two K^+ ions into the already potassium-rich interior of cells, while expelling three Na^+ ions to the sodium-rich extracellular region.[5,6] These gradients of specific ions, and charge more generally, play an important role in regulating numerous downstream biochemical processes. Nature has crafted an inconceivable variety of such molecular machines, which, in a similar fashion, are purpose built to drive highly specific chemical functions at an efficiency which cannot be matched in the laboratory.[2]

Drawing inspiration[7] from these complex biological systems, artificial molecular machines (AMMs) have been developed in an attempt to replicate the precision and efficiency of biochemistry. These AMMs harness an arsenal of non-covalent interactions to direct the motion of molecular components in response to

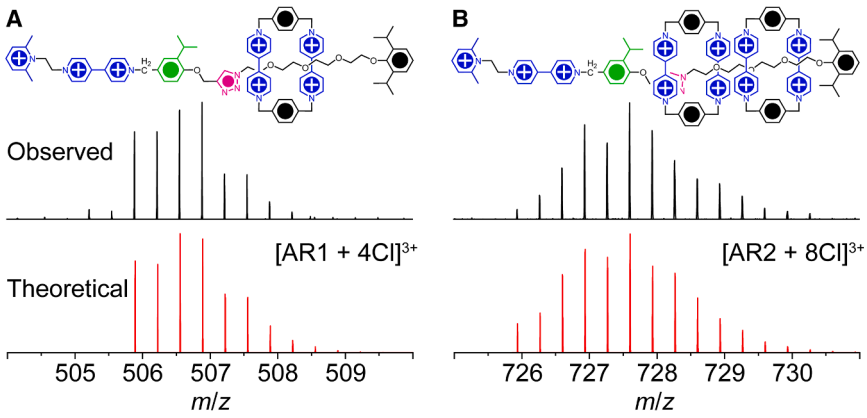

Figure 1. Mass spectra of the rotaxanes produced in water

Evidence for the formation of rotaxanes by the operation of an artificial molecular pump in water from electrospray ionization mass spectrometry (ESI-MS). From top to bottom are the chemical formula, observed isotopic distribution, and simulated isotopic distribution of (A) the [2]rotaxane AR1, and (B) the [3]rotaxane AR2. Presented here are the most abundant intact ions, which demonstrate excellent agreement with the predicted isotopic distributions.

Full spectra are given in the Figures S11 and S17.

external stimulus. In stark contrast to biological molecular machines, which operate exclusively under aqueous conditions, the vast majority of reported AMMs utilize organic solvents. Aqueous AMMs remain exceedingly rare. The scarcity of aqueous AMMs means that their behavior under biologically relevant conditions is poorly understood.

Water presents unique challenges in the design of molecular machinery, including the poor solubility of often lipophilic AMMs,[8] and the irreversibility of redox chemistry for certain commonly employed functional groups.[9] Perhaps more important, however, is the key role that solvent plays in the nanoscale functioning of AMMs.[10] Solvent dictates not only the solubility of a given AMM but also determines the relative strength of supramolecular interactions.[8,11] Water, with its high dielectric constant and capacity to form hydrogen bonds, provides a solvent environment distinct from that of organic media. These properties, which make water indispensable to biology, also mean that the interactions and forces available to drive AMM operation will differ significantly in water compared with more typical solvents.[12,13] For example, competition from water can mute the effects of polar interactions, including hydrogen bonds and donor-acceptor chemistry, often used to drive AMMs in organic solvents.[11] These differences mean that the energy landscape of a given AMM can vary dramatically in water compared with other solvents, impacting both the final product and dynamics of operation. Given the precise balancing act of kinetics and thermodynamics that is AMM design,[3,14–17] the development of aqueous molecular machinery requires an entirely different toolkit.[8,11,18]

Despite these hurdles, water offers unique advantages that could be leveraged to improve AMM performance.[13,19] The ability of water to screen Coulombic interactions, stabilize radicals through solvation effects, and promote hydrophobic aggregation demonstrates that certain interactions are enhanced in aqueous media.[9,19] For example, the π-dimerization of bipyridinium, also called viologen, radicals is significantly favored in water.[19] Recently, with the discovery[20] of the formation of a trisradical tricationic inclusion complex between cyclobis(paraquat-*p*-phenylene) (**CBPQT^{4+}**) and free viologen units, a new generation of radically powered AMMs have been developed in organic solvents.

Among radically driven AMMs, artificial molecular pumps (AMPs) have been extensively studied and developed.[21–25] These radical AMPs take **CBPQT^{4+}** rings from relatively dilute solutions and, driven by formation of the trisradical tricationic complex, accumulate them at higher concentrations on collecting chains, forming rotaxanes. To date, these radical AMPs have all used hexafluorophosphate (PF_6^-) anions in acetonitrile solutions. As both the radical and electrostatic interactions utilized in the operation of these AMPs are applicable in water, with strategic modifications, such a pump could be designed to function under aqueous conditions. In this work, we introduce an AMP that addresses the challenges of altered non-covalent interactions and poor solubility in aqueous media. By employing chloride counterions and a tetraethylene glycol collecting chain to enhance solubility, the system achieves stability and functionality in water. Although these modifications draw upon established design strategies, their successful combination in the context of a working molecular pump marks a significant advance, as translating AMP operation from organic solvents into aqueous media is not trivial. In particular, the aqueous system demonstrates faster kinetics and higher efficiency than its acetonitrile-based counterparts, facilitating the synthesis of [2]- and [3]rotaxanes in high yields as confirmed by NMR spectroscopy and mass spectrometry. See Figure 1. These findings underscore the radically driven AMPs holds substantial potential for integration into biomimetic systems under biochemically relevant environments.

RESULTS AND DISCUSSION

Design and synthesis of an aqueous molecular pump

Current radical-based AMPs are based on the Mark II (MKII^{3+}) pumping cassette, which contains three key functional units: a dimethylpyridinium Coulombic barrier (PY$^+$), a redox-switchable viologen recognition site (BIPY^{2+}), and an isopropylphenylene steric speed bump (IPP)[22] (Figure 2). In basic implementations, this MKII^{3+} pumping cassette is connected to a collecting chain, which is terminated by a bulky stopper unit (S). The MKII^{3+} cassette takes **CBPQT^{4+}** rings from dilute solutions and accumulates them on the collecting chain. Ring movement is driven by modulation of the energy landscape along the length of the pump using redox chemistry. Initially, the cationic ring and pump units are Coulombically repelled. Upon reduction of the viologen units to radicals (BIPY$^{\cdot+}$), the decreased charge of the

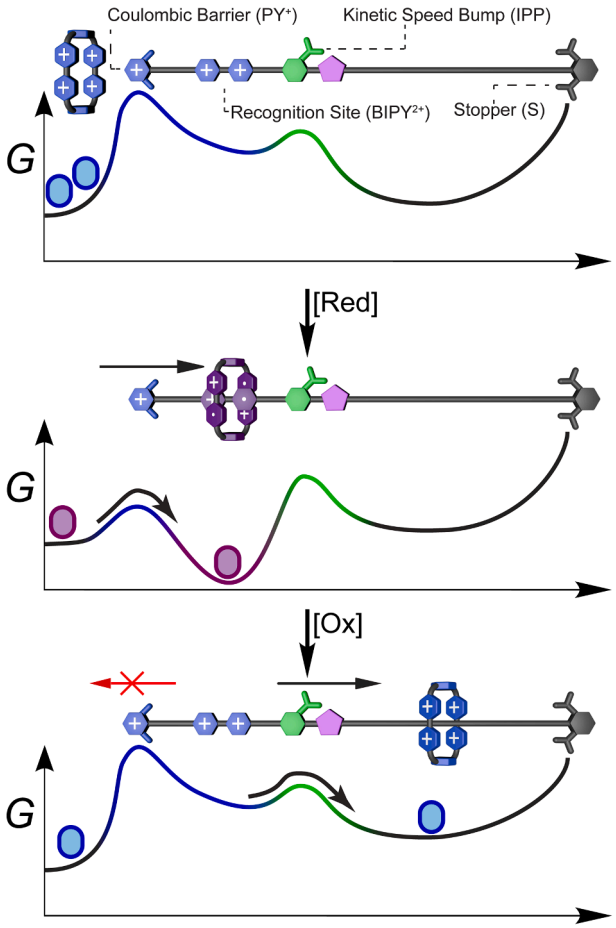

Figure 2. Mechanism of radical pump operation

Labeled graphic depiction of the structure and operating mechanism of a typical, radically powered AMP. The pumping cassette is comprised of a switchable $BIPY^{2+}$ recognition site, between a PY^{+} Coulombic barrier and an IPP steric "speed bump." The cassette is terminated by a collecting chain with a bulky stopper unit. Initially the positively charged **CBPQT^{4+}** ring and pump unit are repelled. Upon reduction, the decreased charge of the **CBPQT$^{2(+)}$** results attenuates the repulsive influence of the PY^{+} barrier, allowing the ring to thread onto the pump to form a trisradical tricationic complex with the recognition site. Oxidation restores the positive charge of both the $CBPQT^{4+}$ and pump, destabilizing the complex. The reinvigorated Coulombic repulsion between the $CBPQT^{4+}$ and PY^{+} barrier prevents dethreading, compelling the ring to traverse the length of the pump, overcome the steric bulk of the IPP unit and become trapped on the collecting chain. During subsequent reduction, the IPP unit prevents return of the trapped $CBPQT^{2(\cdot+)}$ to the recognition site allowing the additional rings to be accumulated from solution.

CBPQT$^{2(\cdot+)}$ rings mutes the repulsion from the PY^{+} barrier, allowing the rings to thread onto the pump forming a trisradical tricationic complex with the $BIPY^{\cdot+}$ recognition site. Oxidation negates the stabilization of the radical complex, compelling movement of the rings, and reinvigorates electrostatic repulsion between $CBPQT^{4+}$ and PY^{+} units, which prevents backward movement. Together, these two effects force the rings to traverse the length of the pump, overcome the steric hinderance of the IPP unit, and come to reside on the collecting chain. During additional redox cycles, threaded rings are prevented from returning to the $BIPY^{\cdot+}$ recognition site by virtue of the steric bulk of the IPP unit, allowing additional rings to be recruited from solution.

A pump (**AP**·3Cl) was designed for operation in water. Structurally **AP**·3Cl comprises a $MKII^{3+}$ cassette, coupled to a tetraethylene glycol-collecting chain, and terminated by a bulky diisopropylphenyl stopper, accompanied by chloride anions (Cl^{-}). These modifications to the design of the $MKII^{3+}$ pump ensure water solubility. The physicochemical properties of viologen salts and their radicals, including **CBPQT^{4+}** rings and many pumping cassettes, are influenced heavily by their counterions.[26–30] In particular, the solubility of these salts is strongly dependent on anions.[26,29,31] Cl^{-} was selected as it is the anion of choice[26] for investigating the radical interactions of $BIPY^{\cdot+}$ units in water, including the demonstration[9] of trisradical tricationic complex formation, which drives the operation of the $MKII^{3+}$. To further enhance solubility, tetraethylene gylcol was used in place of the highly lipophilic oligomethylene collecting chains of previous AMPs.[21,22,25]

The synthesis of **AP**·3Cl was achieved in three steps from known starting materials[22] (Scheme 1). The collecting chain (**AS1**) was prepared by base-driven coupling of tetraethylene glycol monotosylate to diisopropyl phenol via an ether linkage (55%). Azide functionalization of **AS1** with 2-azido-1,3-dimethylimidazolinium hexafluorophosphate (ADMP) afforded **AS2** at 56% yield. Finally, the chain was coupled to the pumping cassette (**PC**·3PF_6) by a copper-catalyzed azide-alkyne cycloaddition, followed by counterion exchange to Cl^{-} salt, yielding **AP**·3Cl quantitatively without chromatography.

Electrospray ionization mass spectrometry (ESI-MS) confirmed the formation of **AP**·3Cl, which could be identified by the unfragmented $[M - 2HCl - Cl]^{+}$ ion with *m/z* of 855.5169, a close match to the theoretical 855.5167. **AP**·3Cl was fully characterized by 1D and 2D NMR. Detailed synthetic protocols and complete spectral data are provided in the supplemental information, see Schemes S1–S3; Figures S1–S5.

Protocol development for pump operation in water

The rigorous selection of redox agents was critical for efficient operation in water. The popular[22,23,25] $CoCp_2$ for reduction and $AgPF_6$ or $NOPF_6$ for oxidation are unsuited to aqueous conditions because of solubility concerns, the possibility of undesired counterion exchange, and reaction with the solvent, respectively. In aqueous media, $BIPY^{2+}$ derivatives (e.g., **CBPQT**·3Cl) are reduced to $BIPY^{\cdot+}$ at approximately −0.45 V and further to neutral $BIPY^{0}$ at −0.88 V vs. NHE.[9,27] While some degree of reduction to the neutral state has been demonstrated to improve the kinetics of AMP operation,[32] in water the second reduction tends to be less reversible than the first, and its products significantly less soluble.[27] To decrease any inefficiencies reducing agents were selected to minimize the production of the "over reduced" species. Metallic iron, zinc, and tetrakis(dimethylamino)ethylene (TDAE) were selected as reducing agents for their compatibility with water, and appropriate redox potentials.[33,34] On the oxidant side, atmospheric O_2 was deemed unsuitable due to the possibility of hydroxide ion production, which can lead to degradation of viologens.[27,35] Ferrocenium hexafluorophosphate ($FeCp_2PF_6$) is a well-known mild oxidizing agent

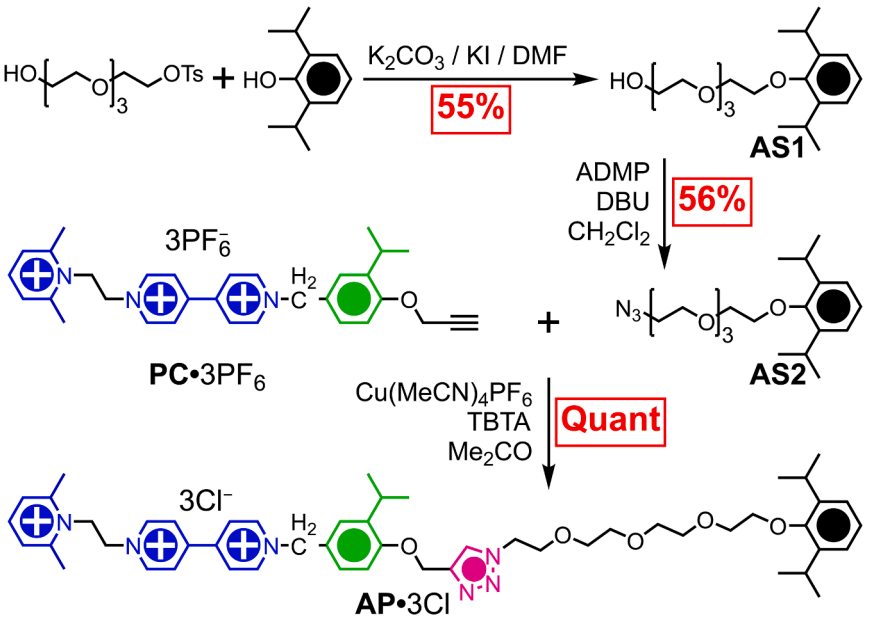

Scheme 1. Synthetic scheme for the water-soluble pump AP·3Cl

Tetraethylene glycol monotosylate was coupled to diisopropyl phenol in DMF to give **AS1** in 55% yield. **AS1** was treated with ADMP and DBU in CH_2Cl_2 resulting in **AS2** at 56% yield. The azide **AS2** was coupled to the pumping cassette[22] **PC**·3PF_6 in Me_2CO with a copper catalyst, followed by counterion exchange to the chloride using tetrabutylammonium chloride (TBACl) in MeCN giving the pump **AP**·3Cl in a quantitative yield.

with demonstrated efficacy for AMP operation[24]; however, it is poorly soluble in water. Instead, its Cl^- salt $FeCp_2Cl$ was selected as it is readily water soluble, simple to prepare,[36] and produces only ferrocene as a waste product, which precipitates from aqueous solutions allowing removal by simple filtration.

The pumping of **CBPQT**$^{4+}$ rings onto the collecting chain of **AP**·3Cl was achieved through sequential redox cycles. In the first instance, the [2]rotaxane (**AR1**·7Cl) was obtained by cycling **AP**·3Cl. Pumping was performed by stirring a solution of 1 mM **AP**·3Cl and a slight excess of **CBPQT**·4Cl with a reducing agent for 30 min under an N_2 atmosphere, see Scheme S4. The heterogeneous metal powders were added in excess and were removed by filtration, while TDAE was added stoichiometrically (0.55 equivalents per $BIPY^{2+}$) and required no filtration. The resultant purple solutions were oxidized by the addition of $FeCp_2Cl$, followed by stirring for a further 30 min to allow the $CBPQT^{4+}$ rings to overcome the IPP steric barrier. Precipitated ferrocene was removed by filtration, and the products were purified by reverse-phase flash chromatography. All three reducing agents gave purified yields exceeding 50%, with TDAE achieving 57%. Formation of **AR1**·7Cl was confirmed by ESI-MS, with the unfragmented $[M - 3Cl]^{3+}$ parent ions measured with an experimental *m/z* of 506.5537 for **AR1**·7Cl compared with the theoretical 506.5555. **AR1**·7Cl was characterized by 1D and 2D NMR vide infra, full assigned spectral data are provided in the supplemental information (Figures S6–S11).

Acquisition of a second ring to produce **AR2**·11Cl required more precise optimization compared with the first cycle. Initial attempts to replicate the conditions of the first cycle for the second resulted in poor purified yields (<5% in the case of iron or TDAE, 0% when using zinc). To understand this decreased yield, UV-vis spectroscopy was employed to identify the radical species present during the reduction of **AP**·3Cl and **AR1**·7Cl. Solutions of $\mathbf{AP}^{\cdot 2+}$, $\mathbf{AP}^{\cdot 2+}$ with $\mathbf{CBPQT}^{2(\cdot+)}$ (1:1), $\mathbf{AR1}^{3\cdot 4+}$, and $\mathbf{AR1}^{3\cdot 4+}$ with $\mathbf{CBPQT}^{2(\cdot+)}$ (1:1) at 1 mM of the pump unit, were prepared by stirring with iron powder for 30 min under an inert atmosphere. The samples were then filtered and sealed in airtight cuvettes (pathlength = 1 mm) for analysis (Figure 3). $\mathbf{AP}^{\cdot 2+}$ alone displays none of the absorptions associated with radical-radical interactions of viologens, indicating that at these concentrations, $\mathbf{AP}^{\cdot 2+}$ exists as monomers in aqueous solution, with π-π dimerization likely disrupted by the presence of the PY^+ unit. In contrast, consistent with the observed ease of production of **AR1**·7Cl, the 1:1 mixture of $\mathbf{AP}^{\cdot 2+}$ and $\mathbf{CBPQT}^{2(\cdot+)}$ exhibits a broad NIR absorption band increasing up to 1,100 nm, which is characteristic[20] of the trisradical tricationic complex required for operation of the $MKII^{3+}$ cassette. On the other hand, $\mathbf{AR1}^{3\cdot 4+}$ instead exhibits an absorption at 860 nm, which is indicative of the presence of viologen π-π dimers.[37] The fact that such radical pairing is not observed for $\mathbf{AP}^{\cdot 2+}$ suggests that the intermolecular interaction is unfavorable, and hence in the case of $\mathbf{AR1}^{3\cdot 4+}$ is likely the result of a folded intramolecular complex. The absence of any trisradical species in the spectra of $\mathbf{AR1}^{3\cdot 4+}$ indicates that the already threaded $CBPQT^{2(\cdot+)}$ rings cannot return to the $BIPY^{\cdot+}$ recognition site during subsequent reduction. Reacquisition of the spectrum of this sample after 24 h corroborates this interpretation, as the resulting spectrum is indistinguishable from that of 30 min post-reduction, eliminating the counter directional movement of rings as a possible explanation for the observed low yields of **AR2**·11Cl. The spectrum of an equimolar mixture of $\mathbf{AR1}^{3\cdot 4+}$ with $\mathbf{CBPQT}^{2(\cdot+)}$ reveals predominantly the dimer band, with a lesser contribution from the trisradical complex. The salience of the dimer band under these conditions suggests that intramolecular radical pairing may out-compete trisradical tricationic complex formation, explaining the poor yield of **AR2**·11Cl. As such, pumping conditions must be optimized to favor trisradical complex formation over dimerization in the second pumping cycle.

Optimization using *in situ* ^1H NMR spectroscopy (details are provided in the supplementary information, see Table S1) found that the use of TDAE with extended reduction times (18 h), elevated concentrations (10 mM **AR1**·7Cl), and greater excesses of **CBPQT**·4Cl (5 equivalents) achieved the desired efficiency. Under these conditions, this second pump cycle was up to 79% efficient prior to purification. When attempted at larger scales, Cl^- salts of **AR2**·11Cl and residual **AR1**·7Cl were poorly

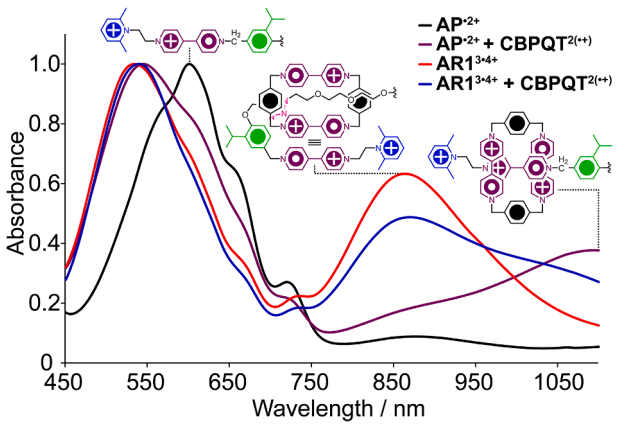

Figure 3. Spectroscopic characterization of radical species

Normalized UV-vis spectra and structures of the radical species responsible for key absorption peaks of **AP**$^{\bullet 2+}$ (black), **AP**$^{\bullet 2+}$ + **CBPQT**$^{2(\bullet+)}$ (purple), **AR1**$^{3\bullet 4+}$ (red), **AR1**$^{3\bullet 4+}$ + **CBPQT**$^{2(\bullet+)}$ (blue). Alone, the pump radical **AP**$^{\bullet 2+}$ exhibits no significant radical interaction bands. The spectra of the [2]rotaxane radical **AR1**$^{3\bullet 4+}$ displays an absorbance at 860 nm which is characteristic[37] of viologen π-π dimers, which can be attributed to an intramolecular interaction between the threaded ring and the BIPY$^{\bullet+}$ recognition site. An equimolar mixture of the, **AP**$^{\bullet 2+}$ + **CBPQT**$^{2(\bullet+)}$, exhibits a broad NIR absorption band increasing up to 1,100 nm, characteristic[20] of viologen trisradical tricationic complexes. The spectra of the combined rotaxane and ring, **AR1**$^{3\bullet 4+}$ + **CBPQT**$^{2(\bullet+)}$, predominantly reveals the dimer band at 860 nm, with the trisradical band being much less intense, indicating that folding and dimerization of the rotaxane dominates over trisradical complex formation in this case, which may inhibit acquisition of a second ring.

separated, which was also the case for chromatography with trifluoroacetic (TFA$^-$) counterions. Anion exchange to PF_6^- proved fruitful, and **AR2**·11PF_6 was isolated in 60% yield after chromatography. Subsequent anion exchange back to the chloride gave **AR2**·11Cl in 88% yield, resulting in a total purified yield of 53%, see Scheme S5. Both **AR2**·11Cl and **AR2**·11PF_6 were identified by ESI-MS, with the $[M - 3Cl]^{3+}$ ion found at *m/z* of 727.6015, and $[M - 3PF_6]^{3+}$ at 1,019.5879 compared with the theoretical values of 727.6017 and 1,019.5912, respectively. **AR2**·11Cl was characterized by 1D and 2D NMR, for full assigned spectra see the Figures S12–S17. This protocol would presumably also be effective for the first pumping cycle, however, given the already high yields of the simpler preparation of **AR1**·7Cl described above, it presents minimal benefit.

Rotaxane characterization and analysis

In line with prior AMP research,[21,22,25] the presence of CBPQT^{4+} rings in **AR1**·7Cl and **AR2**·11Cl results in significant movement in the resonances of their ^{1}H NMR spectra compared with **AP**·3Cl on account of aromatic ring currents (Figure 4). As would be expected, the largest changes in chemical shift occur to the protons directly encircled by, and nearest to the CBPQT^{4+} rings. Comparing the spectrum of **AR1**·7Cl with that of **AP**·3Cl, the peaks of the H-12 of the IPP (green), H-16 belonging to the linker between the IPP and the triazole, H-17 of the triazole unit (pink) substantial upfield movement; from 7.11 to 6.33 ppm, 5.06 to 2.97 ppm, and 7.98 to 5.99 ppm, respectively. While the resonances of the ethylene glycol chain undergo some shifting, it is to a much smaller degree than for similar [2]rotaxanes with oligomethylene collecting chains in CD_3CN.[21,22,25] Taken together, these results suggest that the CBPQT^{4+} in **AR1**·7Cl resides primarily around the triazole unit while in water, presumably the result of hydrophobic interactions.

Similar, though in general far larger changes occur to the ^{1}H NMR spectrum of **AR2**·11Cl compared with that of **AR1**·7Cl, with the second CBPQT^{4+} ring providing additional shielding. The signals from the ethylene glycol protons of the collecting chain resolve into individual resonances ranging from 4.75 ppm to far upfield at 0.86 ppm. In contrast to **AR1**·7Cl, H-17 of the triazole is shifted slightly downfield to 6.57 ppm, while the H-16 linker resonance and H-12 of the IPP are shifted further upfield to 1.72 and 5.30 ppm, respectively. These data indicate that when two rings are present, they will occupy the entire length of the collecting chain. Unlike the broadening observed in comparable charge dense [3]rotaxanes with oligomethylene collecting chains,[21,22,25] the resonances of the CBPQT^{4+} rings remain sharp. The H-α and H-β resonances of the ring closest to the stopper unit (denoted by subscript *S*) exhibit downfield shifts compared with the same protons the other ring (subscript *IPP*) or **AR1**·7Cl. In contrast, H-P_S is located upfield from H-P_{IPP}. These differences can be attributed to the presence of the aromatic triazole unit within the cavity of the ring in **AR1**·7Cl, and the ring nearest the IPP unit in **AR2**·11Cl ($CBPQT_{IPP}$). The face-to-face arrangement of the triazole and BIPY^{2+} units causes shielding to H-α_{IPP} and H-β_{IPP}, moving them upfield, while the side on orientation of the phenylene linker results in deshielding of H-P_{IPP}, shifting it downfield relative to H-P_S. Taken together, the ^{1}H NMR spectra clearly demonstrate the formation of a [3]rotaxane.

These analyses are corroborated by ^{1}H–^{1}H ROESY (rotating-frame nuclear overhauser effect spectroscopy) data. ^{1}H–^{1}H ROESY, which provides insight into through-space interactions, that is their crosspeaks indicate protons, which are located close together. Partial ^{1}H–^{1}H ROESY spectra for **AR1**·7Cl and **AR2**·11Cl are given in Figure 5 focused on the couplings between AP^{3+} and the CBPQT^{4+} rings, full spectra are included in the Figures S9 and S15. For **AR1**·7Cl, the crosspeaks of the collecting chain resonances H-18 to H-23, with H-α, H-β, and H-P of CBPQT^{4+} providing clear evidence for the threading of the ring. For **AR2**·11Cl, the ^{1}H–^{1}H ROESY spectrum is suitably more complex given the presence of the second CBPQT^{4+}; however, the precise arrangement of the two rings is still apparent. Crosspeaks are evident between H-α_{IPP}, H-β_{IPP}, and H-P_{IPP} of $CBPQT_{IPP}$ (marked in green boxes) with H-12, H-14, and H-15 of the IPP, H-16 of the linker, H-17 of the triazole, and the ethylene glycol resonances H-18 to H-20, demonstrating that it resides on the first half of the collecting chain. In contrast, H-α_S, H-β_S, and H-P_S of $CBPQT_S$ (black boxes) exhibit couplings with the glycol peaks H-19 to H-25, as well as with H-27 of the S unit giving clear evidence that $CBPQT_S$ is threaded onto the pump, occupying the second section of the collecting chain and located near to the terminal stopper.

Kinetic analysis of pumping behavior

To better understand the behavior of **AP**·3Cl in water, the kinetics and efficiency of operation were analyzed with *in situ* ^{1}H

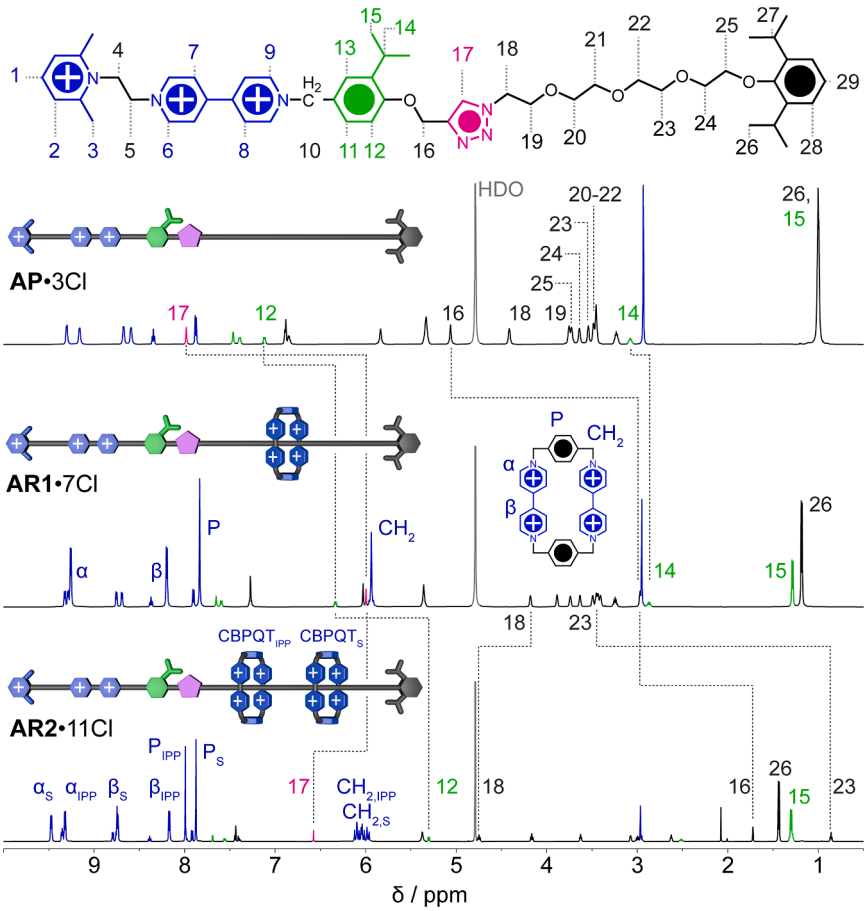

Figure 4. ^{1}H NMR analysis of AP·3Cl, AR1·7Cl, and AR2·11Cl

Comparison of the ^{1}H NMR spectra of (from top to bottom) **AP**·3Cl, **AR1**·7Cl, and **AR2**·11Cl. Spectra were recorded in D_2O at 298 K, at a field strength of 600 MHz. The spectra are color-coded, and the peaks with the most notable changes in chemical shift demonstrating rotaxane formation are labeled. In particular, the presence of a $CBPQT^{4+}$ ring in **AR1**·7Cl results in upfield movement of the peaks for the H-12, H-16, and H-17 protons of the IPP, and collecting chain. These peaks are associated with protons on or near to the IPP unit, indicating the ring in **AR1**·7Cl resides around the triazole unit. The extra ring in **AR2**·11Cl, in addition to the shifting seen for **AR1**·7Cl, also results in movement of the peaks of the H-18 to H-25 protons. This shifting indicates that the two rings in **AR2**·11Cl encircle the entire length of the collecting chain.

NMR spectroscopy. To monitor the kinetics of IPP transit by the $CBPQT^{4+}$ rings, pump cycles were conducted in deoxygenated D_2O, oxidized, and immediately transferred into the spectrometer with spectra recorded periodically. The kinetics can be tracked by monitoring the disappearance of a short-lived intermediate state in which the $CBPQT^{4+}$ resides over the IPP barrier. For **AP**·3Cl in D_2O, at 25°C, no intermediate could be detected in the first spectra recorded after approximately 6 min. In comparison, previous reports[22] of the **MKII**·3PF_6 pump in acetonitrile found the same transition took place much more slowly, requiring approximately 90 min to reach completion at room temperature. Oxidation and analysis at a lower temperature (5°C), and hence decreased rate, allowed detection of the intermediate by ^{1}H NMR as a broad peak centered at 9.40 ppm (see Figure S18). In this case, by the first scan at circa 6 min, IPP transit was already approximately 80% complete, and the intermediate became undetectable 25 min after oxidant addition. The small size and relative broadness of the intermediate peak hindered accurate quantification of the intermediate from, individual spectra as a result of inadequate signal-to-noise. Lowering the temperature further is impractical because of the potential freezing of the sample, so as a remedy, a running average of the integrals over every five spectra was taken to smooth the data. From this averaged data, conversion of the intermediate into **AR1**·7Cl was best fit to a second-order kinetic model (Figure S19), with an apparent rate constant of $k = 10.1 \pm 0.1\ M^{-1}s^{-1}$. In comparison, the rate of IPP transit for the **MKII**·3PF_6 in acetonitrile is reported[22] to follow first-order kinetics as might be expected of what is presumably a unimolecular process, which suggests that this transition is more complex in the case of **AP**·3Cl in water.

Many factors may contribute to this rate enhancement. In this case, the solvent,[8,10,11] counterions,[38–40] and collecting chain composition[41–46] differ, all of which are known to impact the non-covalent interactions that drive such transitions including specifically for $CBPQT^{4+}$-containing compounds.[31] In aqueous environments, the relative strengths of non-covalent interactions differ greatly from organic solvents on account of the high polarity and hydrogen bond forming capacity of water.[8,11] For $CBPQT^{4+}$, complexes assembled by donor-acceptor interactions, which closely resemble the transition state in question are well known, and widely used in AMMs and template-directed syntheses.[31,41] The binding constants for these $CBPQT^{4+}$ donor-acceptor complexes are, in general, reported to be of similar magnitude in water compared with acetonitrile.[31,47] Therefore, while the role of solvent in the observed rate enhancement cannot be discounted, based on the expected similarity in energy levels of the transition state in water and acetonitrile, we propose it is unlikely to be the dominant factor.

Similarly, counterions are known[31,38–40] to impact the host-guest chemistry and dynamic behavior of systems containing $CBPQT^{4+}$. For example, the Jeppesen group has described[40] acceleration of the shuttling rate of a $CBPQT^{4+}$ ring in a [2]rotaxane based switch in the presence of salts of different counterions, an effect which is heightened for smaller anions. As Cl^- used herein is significantly smaller than the PF_6^- anions used for other pumps in acetonitrile, this may partially explain the change in rate. It is difficult, however, to distinguish the impact

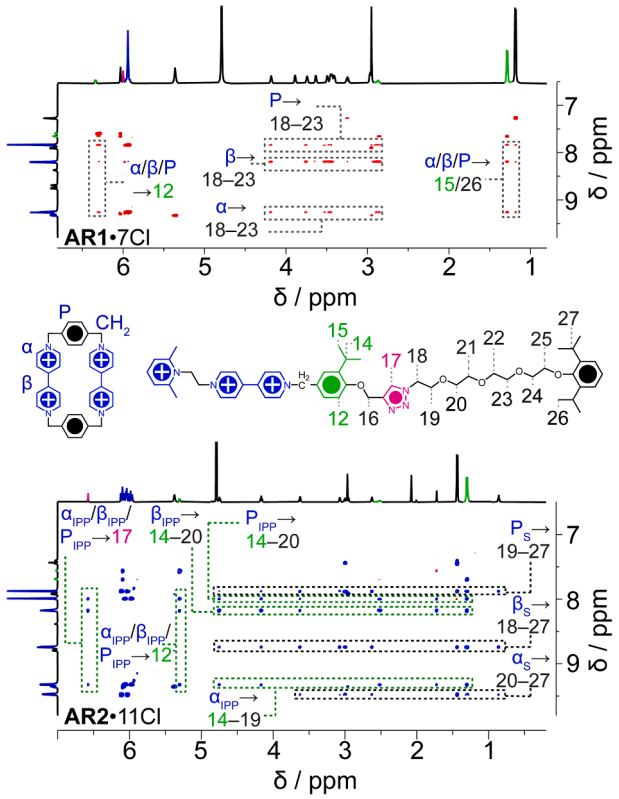

Figure 5. ^{1}H-^{1}H ROESY characterization of the rotaxanes

Partial ^{1}H-^{1}H ROESY spectra (600 MHz, D_2O, 298 K) of **AR1**·7Cl (top) and **AR2**·11Cl (bottom), labeled structures of AP^{3+} and $CBPQT^{4+}$ are given for reference. The key crosspeaks which demonstrate the threading of the rings onto the pump are marked in boxes and annotated. The subscript *S* denotes the $CBPQT^{4+}$ in **AR2**·11Cl located closest to the stopper unit, while the subscript *IPP* denotes the other ring (green boxes). For **AR1**·7Cl, the $CBPQT^{4+}$ protons exhibit crosspeaks with H-12 and H-15 of the IPP, and H-18 to H-23 of the glycol section, confirming that the ring occupies the first section of the collecting chain. For **AR2**·11Cl, the rings can be distinguished as protons $CBPQT_{IPP}$ have clear crosspeaks with H-14 to H-20 belonging to the IPP and first section of the collecting chain, while $CBPQT_S$ exhibits couplings to the H-20 to H-27 protons belonging to the stopper and terminal end of the collecting chain.

of counterions from solvent effects, as anion exchange is commonly used to alter the solvent preferences of $CBPQT^{4+}$ derivatives, as is the case in the current investigation.

While these other factors may indeed contribute to the observed rate increase of IPP transit compared with previous AMPs, we propose that the primary cause is, in fact, the altered end chain composition. It is well established[41,44,48] that glycol chains, because of the gauche effect, can wrap around $CBPQT^{4+}$ to form [C−H···O] hydrogen bonds between the ether oxygens and H-α of the rings. This bonding decreases the energy of host-complexes formed by glycol containing threads and $CBPQT^{4+}$ rings. In this case, the outcome is the stabilization of the transition state in which the ring encircles the IPP unit, which we suggest explains the increased rate. In comparison, the oligomethylene chains of prior AMPs[22] are assumed to have negligible interactions with the rings. Similar behavior was observed[44] in acetonitrile for the dethreading of $CBPQT{\cdot}4PF_6$ rings from [2]pseudorotaxanes in work that may be considered a prototype for radical AMPs. Cheng *et al*. described that, for a [2]pseudorotaxane containing a tetraethylene glycol-collecting chain, ring dethreading was complete after approximately 7 h at 82°C. In comparison, in the case of a [2]pseudorotaxane with an alkyl collecting chain of comparable length dethreading took approximately 16 h at 92°C. Perhaps most convincing, it was found that while ring dethreading for the oligomethylene derivative neatly obeyed first-order kinetics as might be expected, the glycol [2]pseudorotaxane deviated from first-order kinetics. Glycol's key role was confirmed by the observation of an additional rate increase by the addition of free glycol threads. Thus, the active participation of the glycol-collecting chain in the transit of $CBPQT^{4+}$ rings over the IPP unit accounts for both the greatly enhanced rate compared with previous AMPs, and its unexpected reaction order. This explanation further suggests that the enhanced kinetics seen here could also occur if $\mathbf{AP}^{3+}$ were operated in organic solvents like acetonitrile. More work is needed, however, before any conclusion can be made.

Using the same *in situ* ^{1}H NMR data as for kinetics, the efficiency of pump cycling can be ascertained by comparing the proportion of **AR1**·7Cl and residual **AP**·3Cl in a sample. For **AP**·3Cl, pumping efficiency was determined to be 87% when oxidized at room temperature. When oxidation was conducted at 5°C, no residual **AP**·3Cl was detected indicating near quantitative efficiency of conversion to **AR1**·7Cl. In either case, this initial pumping cycle is much more efficient than the second required to produce **AR2**·11Cl at 79% as described above, and superior to **MKII**·$3PF_6$ in acetonitrile which is reported to be 80% efficient.[22]

Conclusion

This work demonstrates the successful design and operation of an AMP capable of efficient function in aqueous environments. The integration of a tetraethylene glycol collecting chain and Cl^- counterions enabled the AMP to overcome the challenges of poor solubility and diminished supramolecular interactions typically encountered in water. The AMP exhibited greatly enhanced kinetics compared with previous iterations in acetonitrile, following second-order kinetics with a rate constant of $10.1 \pm 0.1\ M^{-1}s^{-1}$ at 5°C as confirmed by NMR spectroscopy. Additionally, the pump achieved high efficiency, with purified yields of up to 57% for [2]rotaxane and 53% for [3]rotaxane under optimized conditions. Importantly, translating the operation of radically driven AMPs from organic solvents into water represents a substantial advance, demonstrating that such systems can function effectively under biochemically relevant conditions. These findings indicate that even well-understood AMMs still have much room for development and discovery. By expanding the operational scope of AMPs to aqueous environments, this study provides a foundation for exploring their integration into complex chemical systems.

METHODS

Detailed synthetic protocols, NMR spectra, and ESI-MS data for all compounds are provided in the supplemental methods.

RESOURCE AVAILABILITY

Lead contact

Requests for further information and resources should be directed to and will be fulfilled by the lead contact, Dong Jun Kim (dongjun.kim@unsw.edu.au).

Materials availability

Detailed information about the preparation and characterization of new compounds is provided in the supplemental information.

Data and code availability

This study did not generate any datasets or code.

ACKNOWLEDGMENTS

D.J.K. acknowledges support from the Australian Research Council (DE210101618). The authors acknowledge the Mark Wainwright Analytical Centre at UNSW Sydney. The authors thank Dae Kyung Kim for the valuable assistance in creating the illustrations for the Figures. Also, the authors acknowledge both Northwestern University and UNSW Sydney (Strategic Hires and Retention Pathways) for their financial support of this research.

We dedicate this manuscript to the memory of Prof. Fraser Stoddart, who passed away during the final stages of its preparation. His contributions to this work were made prior to his passing, and we honor his role through this publication.

AUTHOR CONTRIBUTIONS

Conceptualization, C.K.L. and A.E.E.; methodology, C.K.L. and Y.F.; investigation, C.K.L and J.P.V.; writing – original draft, C.K.L., J.F.S., and D.J.K.; writing – review & editing, C.K.L., Y.F., W.A.D., J.F.S., and D.J.K.; funding acquisition, D.J.K.; visualization, C.K.L.; supervision, W.A.D., J.F.S., and D.J.K.

DECLARATION OF INTERESTS

The authors declare no competing interests.

SUPPLEMENTAL INFORMATION

Supplemental information can be found online at https://doi.org/10.1016/j.chempr.2025.102693.

Received: March 6, 2025
Revised: May 26, 2025
Accepted: July 10, 2025

REFERENCES

1. Alberts, B., Johnson, A., Lewis, J., Morgan, D., Raff, M., Roberts, K., and Walter, P. (2015). Molecular Biology of the Cell, Sixth Edition (Garland Science). https://www.routledge.com/Molecular-Biology-of-the-Cell/Alberts-Johnson-Lewis-Morgan-Raff-Roberts-Walter/p/book/9780815344322.
2. Huang, T.J., and Juluri, B.K. (2008). Biological and Biomimetic Molecular Machines. Nanomedicine (Lond) *3*, 107–124. https://doi.org/10.2217/17435889.3.1.107.
3. Pezzato, C., Cheng, C., Stoddart, J.F., and Astumian, R.D. (2017). Mastering the non-equilibrium assembly and operation of molecular machines. Chem. Soc. Rev. *46*, 5491–5507. https://doi.org/10.1039/c7cs00068e.
4. Feng, Y., Ovalle, M., Seale, J.S.W., Lee, C.K., Kim, D.J., Astumian, R.D., and Stoddart, J.F. (2021). Molecular pumps and motors. J. Am. Chem. Soc. *143*, 5569–5591. https://doi.org/10.1021/jacs.0c13388.
5. Skou, J.C. (1957). The influence of some cations on an adenosine triphosphatase from peripheral nerves. Biochim. Biophys. Acta *23*, 394–401. https://doi.org/10.1016/0006-3002(57)90343-8.
6. Skou, J.C. (1998). The Identification of the Sodium-Potassium Pump (Nobel Lecture)Nobel Lecture. Angew. Chem. Int. Ed. *37*, 2320–2328. https://doi.org/10.1002/(SICI)1521-3773(19980918)37:17<2320::AID-ANIE2320>3.0.CO;2-2.
7. Tasbas, M.N., Sahin, E., and Erbas-Cakmak, S. (2021). Bio-inspired molecular machines and their biological applications. Coord. Chem. Rev. *443*, 214039. https://doi.org/10.1016/j.ccr.2021.214039.
8. Oshovsky, G.V., Reinhoudt, D.N., and Verboom, W. (2007). Supramolecular chemistry in water. Angew. Chem. Int. Ed. *46*, 2366–2393. https://doi.org/10.1002/anie.200602815.
9. Li, H., Fahrenbach, A.C., Coskun, A., Zhu, Z., Barin, G., Zhao, Y.-L., Botros, Y.Y., Sauvage, J.-P., and Stoddart, J.F. (2011). A light-stimulated molecular switch driven by radical–radical interactions in water. Angew. Chem. Int. Ed. *50*, 6782–6788. https://doi.org/10.1002/anie.201102510.
10. Di Noja, S., Garrido, M., Gualandi, L., and Ragazzon, G. (2023). Control over Dethreading Kinetics Allows Evaluating the Entropy Stored in an Interlocked Molecular Machine Out-of-Equilibrium**. Chem. Eur. J. *29*, e202300295. https://doi.org/10.1002/chem.202300295.
11. Davis, A.P., Kubik, S., and Dalla Cort, A. (2015). Editorial: Supramolecular chemistry in waterEditorial. Org. Biomol. Chem. *13*, 2499–2500. https://doi.org/10.1039/c5ob90026c.
12. Panman, M.R., Bakker, B.H., den Uyl, D., Kay, E.R., Leigh, D.A., Buma, W.J., Brouwer, A.M., Geenevasen, J.A.J., and Woutersen, S. (2013). Water lubricates hydrogen-bonded molecular machines. Nat. Chem. *5*, 929–934. https://doi.org/10.1038/nchem.1744.
13. Cremer, P.S., Flood, A.H., Gibb, B.C., and Mobley, D.L. (2017). Collaborative routes to clarifying the murky waters of aqueous supramolecular chemistry. Nat. Chem. *10*, 8–16. https://doi.org/10.1038/nchem.2894.
14. Baroncini, M., Silvi, S., Venturi, M., and Credi, A. (2010). Reversible photoswitching of rotaxane character and interplay of thermodynamic stability and kinetic lability in a self-assembling ring–axle molecular system. Chemistry *16*, 11580–11587. https://doi.org/10.1002/chem.201001409.
15. Corra, S., Casimiro, L., Baroncini, M., Groppi, J., La Rosa, M., Tranfić Bakić, M., Silvi, S., and Credi, A. (2021). Artificial supramolecular pumps powered by light. Chemistry *27*, 11076–11083. https://doi.org/10.1002/chem.202101163.
16. Corra, S., Bakić, M.T., Groppi, J., Baroncini, M., Silvi, S., Penocchio, E., Esposito, M., and Credi, A. (2022). Kinetic and energetic insights into the dissipative non-equilibrium operation of an autonomous light-powered supramolecular pump. Nat. Nanotechnol. *17*, 746–751. https://doi.org/10.1038/s41565-022-01151-y.
17. Neira, I., Taticchi, C., Nicoli, F., Curcio, M., Garcia, M.D., Peinador, C., Silvi, S., Baroncini, M., and Credi, A. (2025). Light-driven ratcheted formation of diastereomeric host-guest systems. Chem *11*, 102375. https://doi.org/10.1016/j.chempr.2024.11.013.
18. Murray, J., Kim, K., Ogoshi, T., Yao, W., and Gibb, B.C. (2017). The aqueous supramolecular chemistry of cucurbit[n]urils, pillar[n]arenes and deep-cavity cavitands. Chem. Soc. Rev. *46*, 2479–2496. https://doi.org/10.1039/c7cs00095b.
19. Lee, C.K., Gangadharappa, C., Fahrenbach, A.C., and Kim, D.J. (2024). Harnessing radicals: Advances in self-assembly and molecular machinery. Adv. Mater. *36*, e2408271. https://doi.org/10.1002/adma.202408271.
20. Trabolsi, A., Khashab, N., Fahrenbach, A.C., Friedman, D.C., Colvin, M.T., Cotí, K.K., Benítez, D., Tkatchouk, E., Olsen, J.C., Belowich, M.E., et al. (2010). Radically enhanced molecular recognition. Nat. Chem. *2*, 42–49. https://doi.org/10.1038/nchem.479.
21. Cheng, C., McGonigal, P.R., Schneebeli, S.T., Li, H., Vermeulen, N.A., Ke, C., and Stoddart, J.F. (2015). An artificial molecular pump. Nat. Nanotechnol. *10*, 547–553. https://doi.org/10.1038/nnano.2015.96.
22. Pezzato, C., Nguyen, M.T., Cheng, C., Kim, D.J., Otley, M.T., and Stoddart, J.F. (2017). An efficient artificial molecular pump. Tetrahedron *73*, 4849–4857. https://doi.org/10.1016/j.tet.2017.05.087.

23. Qiu, Y., Zhang, L., Pezzato, C., Feng, Y., Li, W., Nguyen, M.T., Cheng, C., Shen, D., Guo, Q.-H., Shi, Y., et al. (2019). A molecular dual pump. J. Am. Chem. Soc. *141*, 17472–17476. https://doi.org/10.1021/jacs.9b08927.

24. Feng, L., Qiu, Y., Guo, Q.H., Chen, Z., Seale, J.S.W., He, K., Wu, H., Feng, Y., Farha, O.K., Astumian, R.D., et al. (2021). Active mechanisorption driven by pumping cassettes. Science *374*, 1215–1221. https://doi.org/10.1126/science.abk1391.

25. Lee, C.K., Feng, Y., Tajik, M., Violi, J.P., Donald, W.A., Stoddart, J.F., and Kim, D.J. (2024). Concise and efficient synthesis of sequentially isomeric hetero[3]rotaxanes. J. Am. Chem. Soc. *146*, 27109–27116. https://doi.org/10.1021/jacs.4c09406.

26. van Dam, H.T., and Ponjeé, J.J. (1974). Electrochemically generated colored films of insoluble viologen radical compounds. J. Electrochem. Soc. *121*, 1555. https://doi.org/10.1149/1.2401732.

27. Bird, C.L., and Kuhn, A.T. (1981). Electrochemistry of the viologens. Chem. Soc. Rev. *10*, 49–82. https://doi.org/10.1039/cs9811000049.

28. Bhowmik, P.K., Han, H., Cebe, J.J., Burchett, R.A., and Sarker, A.M. (2002). Main-chain viologen polymers with organic counterions exhibiting thermotropic liquid-crystalline and fluorescent properties*. J. Polym. Sci. A Polym. Chem. *40*, 659–674. https://doi.org/10.1002/pola.10134.

29. Bhowmik, P.K., Han, H., Ndedeltchev, I.K., Cebe, J.J., Kang, S.W., and Kumar, S. (2006). Synthesis and characterization of ionic liquids: viologen bis{tetrakis[3,5-bis(trifluoromethyl)phenyl]borate} salts. Liq. Cryst. *33*, 891–906. https://doi.org/10.1080/02678290600871598.

30. Jordão, N., Cruz, H., Branco, A., Pinheiro, C., Pina, F., and Branco, L.C. (2015). Switchable electrochromic devices based on disubstituted bipyridinium derivatives. RSC Adv. *5*, 27867–27873. https://doi.org/10.1039/C5RA02368H.

31. Li, H., Jiao, T., and Shen, L. (2019). Host-guest chemistry of a tetracationic cyclophane, namely, cyclobis (paraquat-*p*-phenylene). Handbook of Macrocyclic Supramolecular Assembly (Springer), pp. 1–33.

32. Jiao, Y., Qiu, Y., Zhang, L., Liu, W.G., Mao, H., Chen, H., Feng, Y., Cai, K., Shen, D., Song, B., et al. (2022). Electron-catalysed molecular recognition. Nature *603*, 265–270. https://doi.org/10.1038/s41586-021-04377-3.

33. Vanysek, P. (2000). CRC handbook of chemistry and physics. Electrochemical Series 8, 8–33.

34. Kuroboshi, M., Tanaka, M., Kishimoto, S., Goto, K., Mochizuki, M., and Tanaka, H. (2000). Tetrakis(dimethylamino)ethylene (TDAE) as a potent organic electron source: alkenylation of aldehydes using an Ni/Cr/TDAE redox system. Tetrahedron Lett. *41*, 81–84. https://doi.org/10.1016/S0040-4039(99)02006-7.

35. Rubio-Presa, R., Lubián, L., Borlaf, M., Ventosa, E., and Sanz, R. (2023). Addressing practical use of viologen-derivatives in redox flow batteries through molecular engineering. ACS Mater. Lett. *5*, 798–802. https://doi.org/10.1021/acsmaterialslett.2c01105.

36. Adams, J.J., Arulsamy, N., Sullivan, B.P., Roddick, D.M., Neuberger, A., and Schmehl, R.H. (2015). Homoleptic tris-diphosphine Re(I) and Re(II) complexes and Re(II) photophysics and photochemistry. Inorg. Chem. *54*, 11136–11149. https://doi.org/10.1021/acs.inorgchem.5b01395.

37. Monk, P.M.S. (1998). Comment on: "Dimer formation of viologen derivatives and their electrochromic properties'. Dyes Pigm. *39*, 125–128. https://doi.org/10.1016/S0143-7208(97)00087-9.

38. Laursen, B.W., Nygaard, S., Jeppesen, J.O., and Stoddart, J.F. (2004). Counterion-induced translational isomerism in a bistable [2]rotaxane. Org. Lett. *6*, 4167–4170. https://doi.org/10.1021/ol048518l.

39. Andersen, S.S., Jensen, M., Sørensen, A., Miyazaki, E., Takimiya, K., Laursen, B.W., Flood, A.H., and Jeppesen, J.O. (2012). Anion effects on the cyclobis(paraquat-p-phenylene) host. Chem. Commun. (Camb) *48*, 5157–5159. https://doi.org/10.1039/c2cc31225e.

40. Andersen, S.S., Saad, A.W., Kristensen, R., Pedersen, T.S., O'Driscoll, L. J., Flood, A.H., and Jeppesen, J.O. (2019). Salts accelerate the switching kinetics of a cyclobis(paraquat-*p*-phenylene) [2]rotaxane. Org. Biomol. Chem. *17*, 2432–2441. https://doi.org/10.1039/C9OB00085B.

41. Asakawa, M., Dehaen, W., L'abbé, G., Menzer, S., Nouwen, J., Raymo, F. M., Stoddart, J.F., and Williams, D.J. (1996). Improved template-directed synthesis of cyclobis(paraquat-p-phenylene). J. Org. Chem. *61*, 9591–9595. https://doi.org/10.1021/jo961488i.

42. Nygaard, S., Hansen, C.N., and Jeppesen, J.O. (2007). Binding studies between triethylene glycol-substituted monopyrrolotetrathiafulvalene derivatives and cyclobis(paraquat-*p*-phenylene). J. Org. Chem. *72*, 1617–1626. https://doi.org/10.1021/jo061962c.

43. Hansen, S.W., Stein, P.C., Sørensen, A., Share, A.I., Witlicki, E.H., Kongsted, J., Flood, A.H., and Jeppesen, J.O. (2012). Quantification of the π–π interactions that govern tertiary structure in donor–acceptor [2]pseudorotaxanes. J. Am. Chem. Soc. *134*, 3857–3863. https://doi.org/10.1021/ja210861v.

44. Cheng, C., McGonigal, P.R., Liu, W.G., Li, H., Vermeulen, N.A., Ke, C., Frasconi, M., Stern, C.L., Goddard, W.A., III, and Stoddart, J.F. (2014). Energetically demanding transport in a supramolecular assembly. J. Am. Chem. Soc. *136*, 14702–14705. https://doi.org/10.1021/ja508615f.

45. Kristensen, R., Andersen, S.S., Olsen, G., and Jeppesen, J.O. (2017). Probing the role of glycol chain lengths in π-donor–acceptor [2]pseudorotaxanes based on monopyrrolo-tetrathiafulvalene and cyclobis(paraquat-*p*-phenylene). J. Org. Chem. *82*, 1371–1379. https://doi.org/10.1021/acs.joc.6b02466.

46. Neumann, M.S., Jensen, S.K., Frederiksen, R., Andersen, S.S., Beck, K. M., and Jeppesen, J.O. (2025). Kinetic studies reveal that the secondary station impacts the rate of motion of cyclobis(paraquat-*p*-phenylene) in out-of-equilibrium rotaxanes. ChemPlusChem *2*, 2500154. https://doi.org/10.1002/cplu.202500154.

47. Venturi, M., Dumas, S., Balzani, V., Cao, J., and Stoddart, J.F. (2004). Threading/dethreading processes in pseudorotaxanes. A thermodynamic and kinetic study. New J. Chem. *28*, 1032. https://doi.org/10.1039/b315933g.

48. Bruns, C.J., and Stoddart, J.F. (2016). The Nature of the Mechanical Bond: From Molecules to Machines (John Wiley & Sons). https://doi.org/10.1002/9781119044123.

Chem

Article

An aqueous artificial molecular pump

Graphical abstract

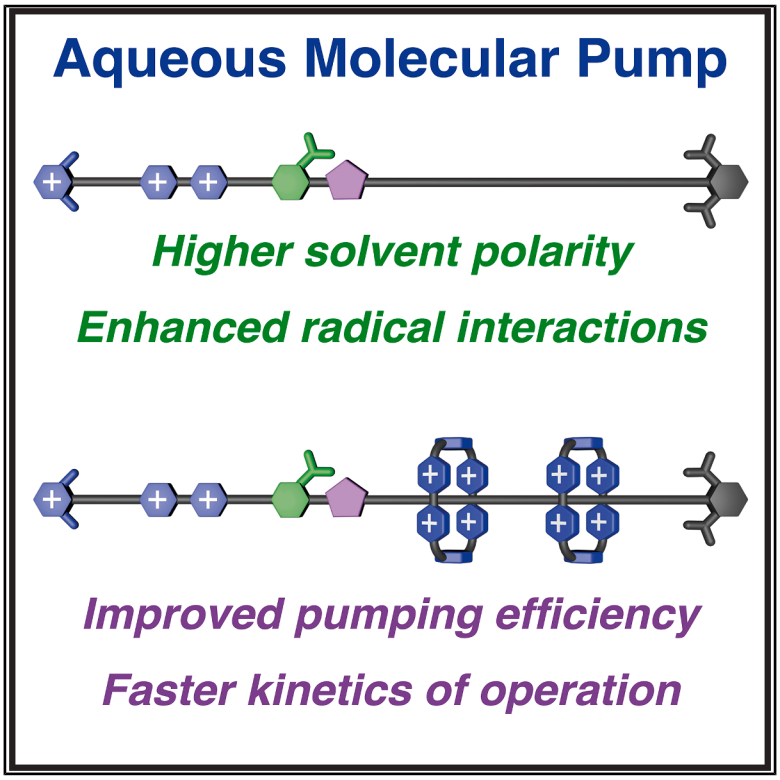

Highlights

- An artificial molecular pump has been designed to operate in water
- Enhanced radical-radical interactions result in high pumping efficiency
- The pump exhibits greatly enhanced kinetics
- Charge-dense rotaxanes have been prepared under aqueous conditions

Authors

Christopher K. Lee, Yuanning Feng, Alan E. Enciso, Jake P. Violi, William A. Donald, J. Fraser Stoddart, Dong Jun Kim

Correspondence

yf@ou.edu (Y.F.), dongjun.kim@unsw.edu.au (D.J.K.)

In brief

An artificial molecular pump has been designed to operate efficiently in water. The polarity of water results in an enhancement to the radical-radical interactions, which drive operation, resulting in enhanced pumping efficiency. Using this pump, [2]- and [3]rotaxanes have been made under aqueous conditions in high yield. This is a rare example of an artificial molecular machine, that operates in water, unlocking the potential for its integration into the myriad complex supramolecular systems which exists in aqueous environments.

Lee et al., 2026, Chem *12*, 102693
January 15, 2026
https://doi.org/10.1016/j.chempr.2025.102693

CellPress